

*Full length article***PETROGRAPHIC AND SEM-EDX CHARACTERIZATION OF MAFIC-FELSIC PLUTONIC ROCKS OF WASHAPI KAUR WESTERN RASKOH ARC, PAKISTAN**Jafer Iqbal<sup>1</sup>, Inayat Ullah<sup>1,\*</sup>, Razzaq Abdul Manan<sup>1</sup>, Abdul Ghaffar<sup>1</sup>, Fida Murad<sup>1</sup>, Jalil Ahmed<sup>2</sup>

1. Centre of Excellence in Mineralogy, University of Balochistan, Quetta 87550, Pakistan

2. Department of Geology, University of Balochistan, Quetta 87550, Pakistan

**ABSTRACT**

The Washapi Kaur plutonic rocks is located at the western part of the Ras-Koh arc, Pakistan, and intruded in the Cretaceous to Paleocene rock sequences. This complex consists of two main magma series, mafic to intermediate, forming small gabbro and diorite intrusions and felsic comprising granitic rock units. Gabbro consists of clinopyroxene, plagioclase, amphibole, and biotite and displays in-equigranular poikilitic texture. Diorites present porphyritic texture and mainly composed of plagioclase, K-feldspar, amphibole, quartz, and biotite with minor constituents of clinopyroxene. Granites are comprised of quartz, K-feldspar, plagioclase, biotite and muscovite. The field features, petrographic and SEM (Scanning Electron Microscopy) suggest that the magmatic activity in the Washapi Kaur formed as the initial mantle-melt magma derived from mafic to the intermediate source. Later, the melt interacted with slab-derived hydrous fluids in a continental arc setting.

**KEYWORDS:** Igneous intrusions, Calc-alkaline, Ras-Koh arc, Pakistan\*Corresponding author: (Email: [inayat.cem@um.uob.edu.pk](mailto:inayat.cem@um.uob.edu.pk))**1. INTRODUCTION**

Igneous intrusions with mafic to silicic composition composed of gabbro, diorite, granodiorite and granite are formed by the mantle magma and partial melting of continental crust (1, 2, 3). These igneous complexes tectonically occur in the crustal extension, rifting zone, hot spot within the plate, along the subduction zone and orogenic belt. The petrological and geochemical characteristics of felsic igneous intrusions are conclusively described by mixing mafic magma with the crustal melt. Therefore, the diorite and granitic rock units are predominant in the mafic-silicic layer intrusion, indicating the evidence of upward fractional crystallization of the episodic variation of gabbroic intrusion (4, 5, 6, 7). Granitic intrusion formed by the partially melting of continental crust is a basic process that physically stabilizes and chemically discriminates the continental crust. Evaluating

the temperature and pressure of the partially melt of continental crust plays a key role in understanding the genesis of granitic intrusion (8, 9). According to Clemens et al. (2020), the granitic intrusions are formed by the residual melting of granulitic rock units, and emplacements form the shallow continental crust (10).

The Chagai and Raskoh magmatic arcs are Jurassic to Paleocene in age and are theolitic, which developed in response to Neo-Tethyan intra-oceanic subduction to continent-arc collision in western Pakistan. Whereas post-Paleocene intrusive rocks generated in an Andean-arc system (12). Raskoh intrusions are, well developed composed of mafic to felsic rock units (13). These intrusive formed batholiths (Raskoh and Koh-i-Kambran Batholiths), several laccoliths, small intrusive stocks, dikes and sills. These intrusive structures intruded older (Cretaceous) rock sequences, i.e., Kuchaki and

Rakshani Formations in the Raskoh range. Previously, there were no detailed petrographic or geochemical studies on these intrusive bodies. This situation hinders understanding the magmatic and petrographic evolution of Raskoh intrusions and more specifically Washapi Kaur plutonic rocks. This article is focused on the geological field features, petrography, and major geochemical characteristics of the Washapi Kaur intrusions.

## 2. REGIONAL GEOLOGY

The Raskoh arc strikes from north-east to southwest direction about 250 km long, and 50 km wide zone mainly consist of accretionary complex mélangé, ophiolitic rock unit, volcanic-sedimentary sequence, intra-oceanic arc unit associated with granodioritic intrusion covered by the tertiary to quaternary sedimentary rock units (Fig.1; 14). This arc is well-known as the frontal arc of the Chagai arc (12, 15). Regionally, the Ras-Koh arc is part of the Makran-Trench arc system. Both Chagai and Ras-Koh formed a double-arc (Chagai-Raskoh arc) system, which is separated by Dalbandin Trough (13, 11). Ras-Koh arc develops south of the Chagai arc, whereas its eastern boundary ends at the Noshki-Chaman transform fault system. The northward subduction of the Neo-Tethyan ocean extensively develops the Ras-Koh arc underneath the southern part of the Afghan block (16, 17, 18), whereas, considered as the accreted mass of an oceanic island arc (19, 20, 21, 14).

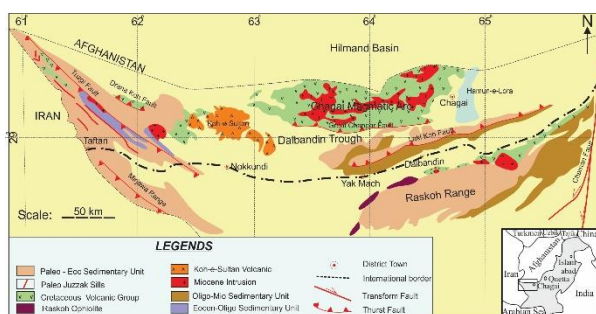


**Figure 1.** Regional geology and tectonic map of Ras-Koh arc, representing the various lithological units and Ras-Koh ophiolite in the region (13).

The Bunap mélangé is the oldest rock unit (late Jurassic to early Cretaceous) in the Ras-Koh arc,

which has thrust contact with the overlying Ras-Koh ophiolite (Bunap Massif in Bunap area), an early to middle Jurassic Radiolarian chert unit and late Jurassic Sedimentary complex (22). This mélangé unit was emplaced on the Neo-Tethyan Oceanic floor between the passive northern margins of Gondwana landmass and the southern part of the Afghan block (22). The overlying Bunap massif of Raskoh ophiolite is comprised of metamorphic sole rock, peridotite, dunite, pyroxenite, gabbro cumulates, and pillow lava basalt with minor chert (21, 14). The Late Cretaceous Kuchaki Formation is most exposed lithological unit in the study area, mainly consisting of basaltic to andesitic lava flows and their pyroclastic equivalents, with thin-bedded limestone, sandstone, mudstone, and chert (13). The Paleocene Rakshani Formation is comprised of sandstone and shale, with minor basalts. The lower and of Rakshani Formation is disconformable with the Ras-Koh Ophiolite. The Raskoh intrusion was dated  $40\text{Ar}-39\text{Ar}$ , the dating results of biotite and hornblende indicated the Ras-Koh intrusions were cooled about  $\sim 48 - 46 \text{ Ma}$  (21). The Eocene Kharan Limestone predominantly consists of thick-bedded to massive bioclastic limestone intercalated with argillaceous limestone and has conformable contact with overlying Oligocene Nouroz Formation (13).

## 3. GEOLOGY OF THE WASHAPI KAUR

### 3.1. PLUTONIC COMPLEX

The Washapi Kaur plutonic complex is located in the western part of the Ras-Koh arc, approximately 15 to 20 km southwest of Dalbandin town. These intrusions are widely dispersed as a small stock and have intrusive contact with the Late Cretaceous Kuchaki Formation (Fig.2). The Washapi Kaur intrusion is composed of gabbro, diorite, and granitic. Gabbro and diorite are formed in the central part of the intrusion, whereas granitic units are formed as dyke and lenticular sills (Fig.3).

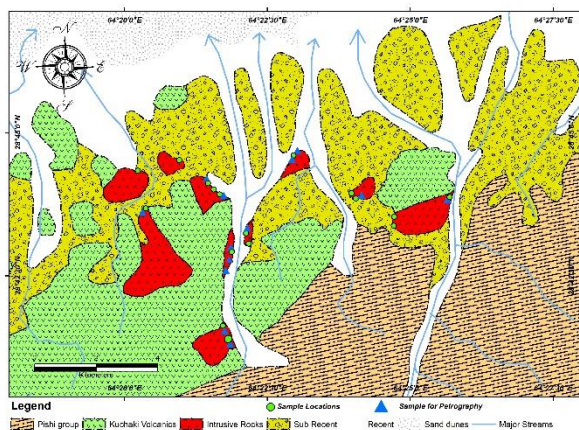


**Figure 2.** Geological map of the study area.

Granitic intrusions are present in small stock, dyke and sill in the study area (Fig.3). Granite has coarse grain texture; the fresh color is light reddish weather's reddish-brown to dark brown. The granitic unit is mainly in contact with the dioritic, basaltic unit and the biotite pegmatite (Fig.3). These units display intense fractures with the spheroidal type of weathered surface (Fig. 4a, b). Biotite pegmatite in the study area intruded within the granitic intrusion (Fig. 4c, d).

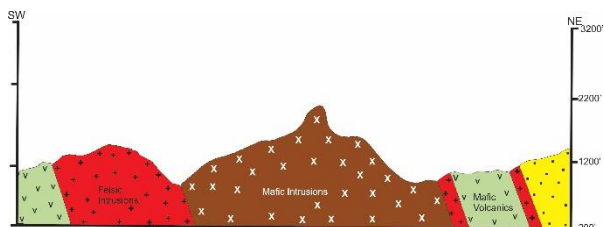


**Figure 3.** Generalized cross-section showing the mafic-felsic intrusive rocks of Washapi Kaur are.

Biotite pegmatite in the study area intruded within the granitic intrusion (Fig. 4c, d). The shape of biotite pegmatite in the study area looks like a dome shape (Fig.4c, d). Gabbro and dioritic intrusion mainly consist of ferromagnesian minerals like pyroxene, amphibole and biotite. Very coarse grains of biotite and plagioclase with laths crystal structure visible with a naked eye are mainly predominant in these intrusions. The peripheral part of these intrusions shows a significant variation in texture and composition because of intense weathering; the chlorite and epidote alteration is pervasive (Fig.4e, f).

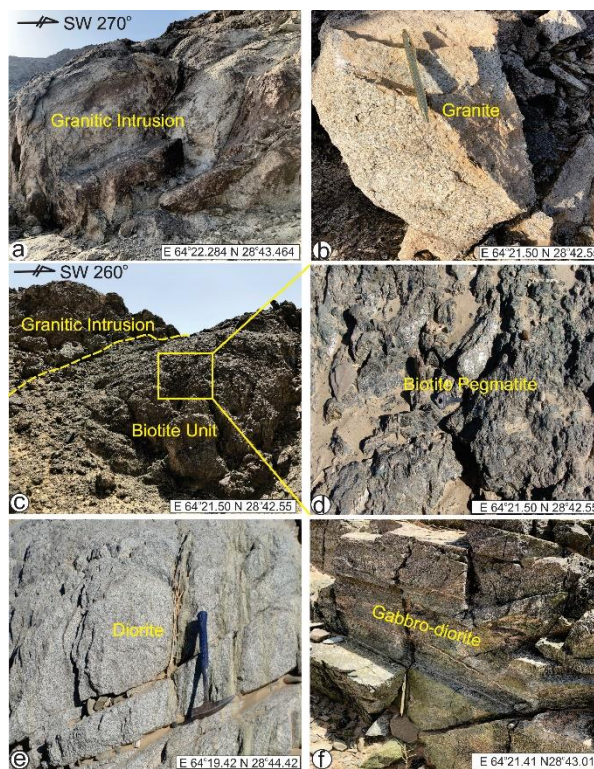


**Figure 4 (a – f).** The field photographs represent the Different intrusions with numerous features. (a and b) Spheroidal weathering of granitic intrusions with the intensely light and dark brown color weathered surface of granite and fresh surface of granite is a light color with a coarse grain texture. (c and d) The dome shape of biotite pegmatite intruded within the granitic rock units, the biotite pegmatite has coarse grain well developed flaky or sheet-like crystal structure. (e) Light color dioritic intrusion has a coarse grain texture with black biotite and amphibole well-developed grain cut across the green epidote vein. (f) Dark grey to grey color weathered surface of gabbro to gabbro diorite intrusion has coarse grain texture with green color intense chlorite alteration.

#### 4. ANALYTICAL METHODS

Thin sections were prepared and examined with an optical (Leica DM 500) binocular microscope, which was further refined with Scanning Electron Microscope at the Centre of Excellence in Mineralogy, University of Balochistan CEM-UOB, Quetta. A Scanning Electron Microscope – Energy Dispersive X-ray spectrometer (SEM-EDX) equipped with a Back Scattered Electron (BSE) imaging unit were used to study the major mineralogical composition and texture of the samples at the laboratory of CEM-UOB, Quetta. The SEM analysis of ten least

altered samples were selected and performed in a SEM Model: JSM- IT 200 coupled with EDS for major oxides. Small chips were taken out from the rock, subsequently polished and coated with gold to obtain BSE imaging and EDX results. For the operational conditions we used an electron current = 90  $\mu$ A, a constant acceleration voltage = 18 kV, and a work distance = 15 mm. We analyzed seven spots on feldspar, seven spots on clinopyroxene, ten spots on amphibole and ten spots on biotite. The result of major oxides are presented in Table.1 and mineral analysis in Table. 2.

## 5. PETROGRAPHY

Gabbro rock units are mainly composed of essential minerals calcium-rich plagioclase (anorthite) (44.03 vol. %), clinopyroxene (21.12 vol. %), amphibole (11.02 vol. %), biotite (10.03 vol. %) and the presence of minor constituents of k-feldspar (2.58 vol. %). The accessory minerals comprised of zoisite, rutile, chromespinel and opaque, whereas low-grade metamorphic minerals include prehnite and pumphilite. The secondary minerals are predominantly enriched with chlorite, epidote and sericite, these are alteration product of clinopyroxene, amphibole, biotite, plagioclase and k-feldspar. The gabbro-diorites have sub-ophitic to interlocking texture among the clinopyroxene and plagioclase grains. In Wk-04, Wk-11-1 and Wk-13-2 the plagioclase, biotite and clinopyroxene have coarse grain texture with laths crystal structure bounded by the chlorite and sericite. Some samples display inequigranular, poikilitic texture. (Figs. 5a – f and 9a – h).

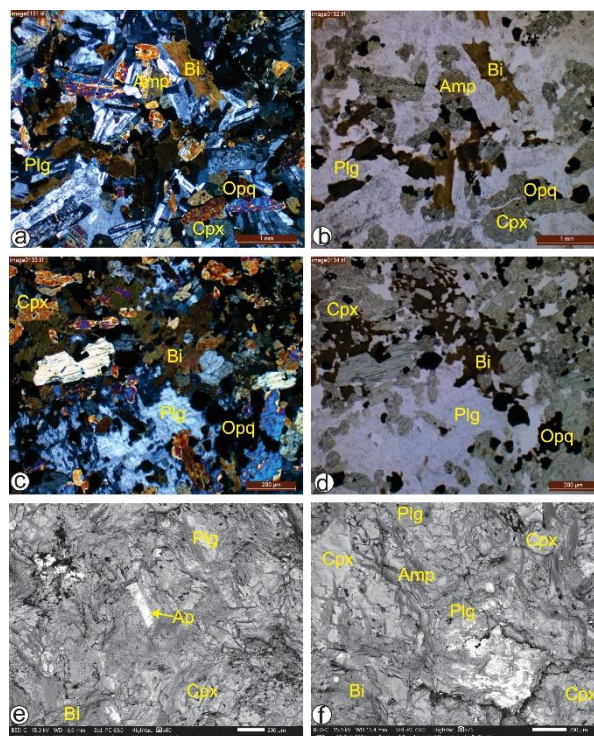


**Figure 5.** (a – d); a and c XPL, b and d PPL; 2.5X) Photomicrograph showing the petrographic feature of the gabbro rock unit is chiefly composed of clinopyroxene, calcium-rich plagioclase (anorthite), amphibole and biotite with equigranular and poikilitic texture. (e – f) BSE images illustrate the texture and compositional variation of gabbro. Abbreviations: Cpx, Clinopyroxene; Plg, Plagioclase; Amp, Amphibole; Bi, Biotite; Ap, Apatite; Opq; Opaque; Mag, Magnetite; Cross Polarized Light; PPL, Plane Polarized Light.

Diorites are predominantly composed of quartz (44 vol. %), plagioclase (26 vol. %), k-feldspar (12 vol. %), biotite (11 vol. %) and amphibole (8 vol. %) with minor clinopyroxene (4 vol. %) constituents and accessory apatite, zircon, ilmenite, sphene and opaque minerals. This rock unit has a porphyritic texture with phenocrysts of quartz, plagioclase, k-feldspar, clinopyroxene having groundmass of the same minerals (Fig. 6 a – f).

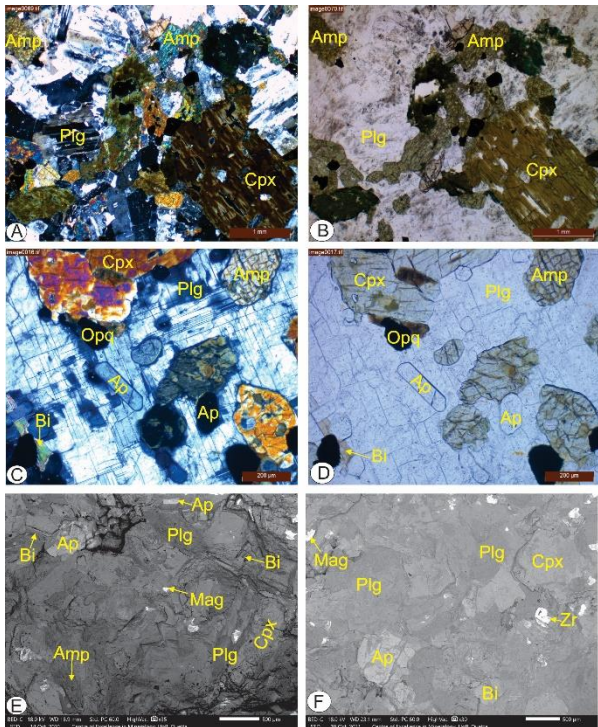


**Figure 6.** (a – d); a and c XPL, b and d PPL; 2.5X) Photomicrograph showing the petrographic feature of the diorite rock unit is chiefly composed of clinopyroxene, calcium rich plagioclase (anorthite), amphibole, biotite and accessory minerals apatite with inequigranular and ophitic texture. (e – f) BSE image illustrate the texture and compositional variation of diorite. Abbreviations: Zr, Zircon; other abriviations in Fig. 5.

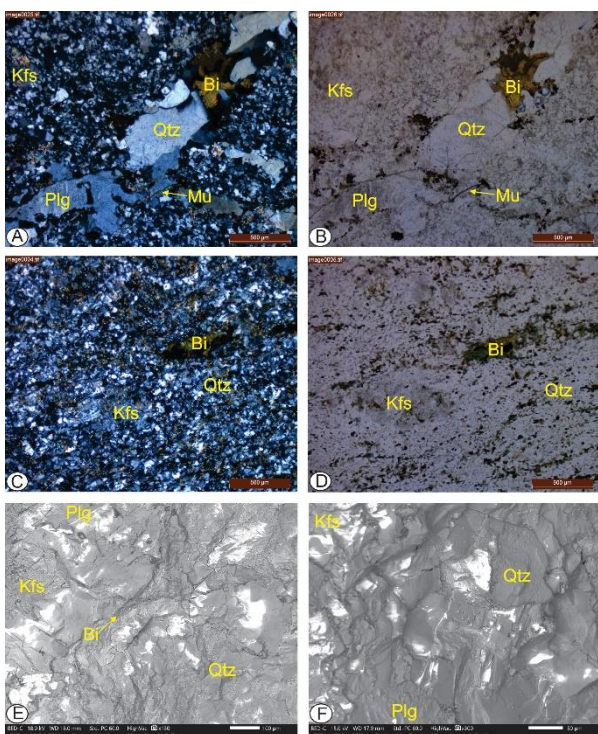


**Figure 7.** (a – d); a and c XPL, b and d PPL; 2.5X) Photomicrograph showing the petrographic feature of the granitic rock unit consists of quartz, k-feldspar, albite plagioclase, biotite and muscovite with fine to medium grain texture because of micro-granular texture indicated the micro-granite. (e – f) BSE image illustrates the texture and compositional variation of granite. Abbreviations: Kfs, K-feldspar; Mu, Muscovite; Qtz, Quartz, other abriviations in Figs.5 and 6.

Granite consist of quartz (69 vol. %), k-feldspar (13 vol. %), albite plagioclase (8 vol. %), biotite (7 vol. %) and muscovite (3 vol. %) associated with accessory minerals, apatite, zircon and opaque minerals. This rock unit has medium grain texture of quartz, plagioclase, k-feldspar, biotite and muscovite because of fine to medium grain texture, the granitic rock is called micro-granite (Figs. 7a – f and 8 i – p).

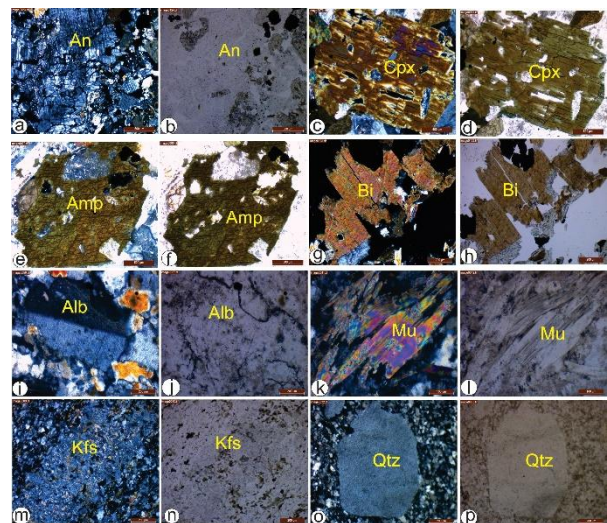


**Figure 8.** (a – b) Plagioclase has a type of calcium-rich anorthite plagioclase, thin lamella coarse grain texture, and euhedral well developed elongated laths crystal structure. (c – d) Clinopyroxene has pale brown, brown, pale green and pink color, medium to coarse grain texture with sample and a lamellar twin along the composition plane and moderate to high relief. (e – f) Amphibole has high order interference figure with pale green to pale brown color, medium to coarse grain texture and double set perfect cleavages. (g – h) Biotite has pale brown to green color, medium to coarse grain texture, flaky crystal structure with highly perfect cleavages and highly pleochoric and moderate relief. (i and j) K-feldspar has white interference color, medium to coarse grain texture, euhedral to subhedral crystal shape with sample twinning. (k – l) Muscovite has pale green to

pink color, a medium to coarse grain texture, and a flaky crystal structure with perfect cleavage. (m – n) Plagioclase has medium to coarse grain texture, subhedral to euhedral crystal shape and polysynthetic albite twinning with medium to thick lamellas. (o – p) Quartz has coarse grain inequigranular texture, subhedral to euhedral prismatic crystal structure with undulose extinction. Abbreviations: An, Anorthite; Alb, Albite, other abbreviations in Figs.5, 6 and 7.

### 5.1 Petrographic/textural variations in Washapi Kaur intrusions

The significant constituents of gabbro are calcium-rich anorthite plagioclase and clinopyroxene. Therefore, the calcium-rich plagioclase (anorthite) is characterized by the thin lamella that occurred along the twinning plane and section no Wk-11-1 consists of thin percales-albite type polysynthetic twinning. Anorthite plagioclase has characterized by coarse grain texture, euhedral well developed elongated laths crystal structure with white to first-order interference color in cross-polarized light and plane-polarized light anorthite plagioclase has colorless interference figure with moderate to low relief (Fig.9 a, b). Clinopyroxene has second to third order high interference figure with pale brown and brown, pale green and pink color, medium to coarse grain texture, subhedral to euhedral crystal shape with sample and a lamellar twin along the composition plane, perfect cleavage and irregular fracture with incline extinction along the cleavage plane in cross-polar light. Clinopyroxene has high interference color greenish to light brownish pleochroic image with moderate to high relief (Fig. 8c, d).

The diorite units are highly dominant amphibole, biotite and sodium rich plagioclase. Amphibole has second to third-order interference figure with pale green to pale brown color, medium to coarse grain texture, double set perfect cleavage with subhedral to euhedral well developed prismatic crystal structure. Amphibole grains look like a biotite grain elsewhere the major difference is cleavage angle, the amphibole has double set perfect cleavage and biotite has single set parallel

cleavage (Fig.7. e and f). Biotite has pale brown to green interference color, medium to coarse grain texture, and a flaky crystal structure with perfect cleavages. Lath crystals of biotite have bird eye extinction with highly pleochroic and moderate relief in the plane-polarized light (Fig. 8g, h).

The granitic rock unit mainly consists of quartz, k-feldspar, sodium rich plagioclase albite, biotite and muscovite. Muscovite has pale green to pink interference color, medium to coarse grain texture, and a flaky crystal structure with perfect cleavages. The orthoclase type of k-feldspar is chiefly dominant in this rock units. First order to white interference color, medium to coarse grain texture, euhedral to subhedral crystal shape with sample twinning in cross-polarized light, colorless interference figure, and low moderate relief in plane-polarized light. Sericitization is more common in Wk 02-1 and Wk 05-3, therefore, the sericitization is an alteration product of orthoclase feldspar (Fig.8 i, j). Lath crystals of muscovite is highly pleochroic and moderate relief in the plane polarized light. Muscovite is commonly altered into chlorite in Wk 12 and Wk 05-3 section (Fig.8 k, l). Plagioclase has medium to coarse grain texture, subhedral to euhedral crystal shape, polysynthetic albite twinning with medium to thick lamellas and laths crystal structures with low interference color in cross-polarized light. In Wk 03-2, Wk 10-2 and Wk 19-2, the core of plagioclase grains are partly altered into sericite and epidote. The fine grain sphene and apatite grains are included within the plagioclase grains (Fig.8 m, n). Quartz is highly dominant in the granitic rock unit. Quartz has fine to coarse grain inequigranular texture, subhedral to euhedral prismatic crystal structure with undulose extinction and colorless to low interference color with negative relief. (Fig.8 o, p).

## 6. RESULTS

### 6.1 Major Elements Geochemistry

SEM-EDX results for major oxides of intrusive rocks of Washapi Kaur intrusions are slight variant in SiO<sub>2</sub> (51.19-77.75 wt%), Al<sub>2</sub>O<sub>3</sub> (14.21- 18.9 wt %), K<sub>2</sub>O (0.56 – 1.67 wt%), Na<sub>2</sub>O (2.03 – 4.4. wt %),

CaO (0.2–12.97 wt%), MgO (0.2–6.98 wt%), FeO (0.45–9.89 wt%), MnO (0.03–0.23 wt%), P<sub>2</sub>O<sub>5</sub> (0.24 wt%–0.93 wt%) and TiO<sub>2</sub> (0.06–0.95 wt%) (Table.1).

In the discrimination diagram, the intrusive rocks are classified as gabbro-diorite, diorite, and granite in the silica versus total alkalis diagram (Fig. 9; 24). In the SiO<sub>2</sub> versus K<sub>2</sub>O (25), both mafic and felsic intrusion of Washapi Kaur complex fall in the calc-alkaline field, which indicates calc-alkaline type magmatism for Washapi Kaur complex (Fig. 9).

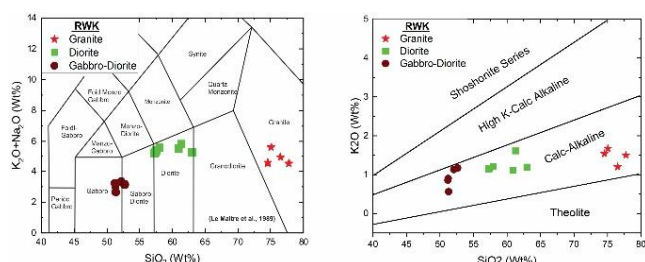


**Figure 9.** Discrimination binary diagram illustrate the total alkali versus SiO<sub>2</sub> of studied rocks in the study area (24; 25).

## 7. DISCUSSION

### 7.1 Petrographical evidence for magma evolution

Petrographically the Washapi Kaur the intrusive rocks are composed of mafic to felsic and identified as gabbro, diorite and granite. The plutonic contact between dioritic and granitic rock units are intensively sharp with visible effects of chilling (Fig. 4), which is indicate the late phase of magmatic intrusion of granite within the dioritic intrusion. The gabbro to gabbro-diorite and diorites are consist of high constituents of hydrous minerals such as amphibole and biotite, tectonically which is indicated that the starting of early phase of oceanic plate subduction beneath the continental plate with high contamination of the oceanic plate and the granitic rock units having dominant felsic phases such as quartz, alkali feldspar and plagioclase, tectonically that is indicate the genesis of granitic rock units are linked with high involments of continental plate.

### 7.1.1 Feldspar: Types and Origin

The plagioclase grains change from calcium-rich plagioclase (An) to sodium-rich plagioclase (Alb) in gabbro-diorite to granites (Table. 2). The plagioclase grains core in gabbro-diorite and diorite rock mainly consists of calcium-rich plagioclase (Anorthite-Bytownite), while rims with andesine compositions. These compositional changes represents hybrids mafic to felsic magma types; typically, the patchy zone anorthite and bytownite core are resorbed and overgrowth by the Ca-Na rich plagioclase andesine rims. The Ca-rich core plagioclase (An) is crystallized from the mafic type magma and the early phase of felsic magma feeds from the acidic magma chamber (26, 27).

Strong undercooling in the mafic magma infiltrated the more acidic magma may have led to the formation of unusual dendritic and boxy-cellular calcic plagioclase crystals with patchy zoning (5, 28, 29). Rare crystals of andesine (early-formed crystals acquired from the acidic magma) would have been melted and partially resorbed in the hybrid dioritic magma before being overtaken by a limited zone of Ca-rich plagioclase. Crystallization would have evolved slowly after mixing and thermal readjustment, changing the plagioclase from thin calcic zones to broad zoned andesine rims. At the same time, the comparatively sodic core would have overgrown the more typical calcic cores, while tiny, unzoned plagioclase of similar composition nucleated and formed in the groundmass (30, 31). The Ca-rich, Ca-Na rich and Na rich plagioclase were observed in the gabbro-diorite, diorite and granitic rock units in Washapi Kaur intrusive complex (Fig. 10 a, b). Therefore, the compositional variation of plagioclase feldspar generally describes the feeding of the magma chamber with new pulses of magma in Washapi Kaur intrusion.

**Table 1.** Major Oxides of mafic-felsic rocks from Washapi Kaur Complex, Ras-Koh arc.

Elements	Major Elements Geochemistry Results															
	Granite				Diorite								Gabbro Diorite			
	wk2-1	wk5-3	wk5-4	wk12-1	wk03-2	wk19-1	wk03-1	wk15-2	wk10-1	wk15-1	wk19-2	wk00-2	wk01-1	wk13-1	wk11-1	wk4-1
<b>SiO<sub>2</sub>%</b>	77.75	76.51	75.06	74.54	62.98	61.28	60.88	57.95	57.45	57.3	57.23	52.63	52.06	51.3	51.23	51.19
<b>Al<sub>2</sub>O<sub>3</sub>%</b>	14.21	16.79	15.91	17.82	14.85	16.24	18.9	15.65	15.24	14.85	15.84	15.62	17.74	14.36	17.6	17.16
<b>K<sub>2</sub>O%</b>	1.5	1.2	1.67	1.54	1.19	1.61	1.11	1.2	1.16	1.13	1.16	0.87	0.73	0.56	0.9	0.86
<b>Na<sub>2</sub>O%</b>	3.03	3.72	3.92	3.02	4.1	4.23	4.42	4.4	4.27	4.14	4.1	2.03	2.23	2.13	2.16	2.42
<b>CaO%</b>	0.9	0.2	1.08	1.13	4.57	5.84	4.13	8.7	7.35	8.88	6.42	12.97	11.85	12.29	11.97	11.86
<b>MgO%</b>	0.5	0.2	0.9	0.42	3.5	3.92	3.14	3.91	4.19	5.11	5.44	5.83	5.95	6.98	6.94	5.63
<b>FeO%</b>	0.65	0.48	0.45	0.37	6.85	5.27	6.03	5.74	8.25	7.01	8.19	8.02	7.17	9.89	6.74	9.04
<b>MnO%</b>	0.21	0.03	0.06	0.05	0.18	0.08	0.03	0.11	0.23	0.08	0.15	0.21	0.27	0.09	0.21	0.21
<b>P<sub>2</sub>O<sub>5</sub>%</b>	0.26	0.24	0.35	0.36	0.45	0.41	0.53	0.56	0.66	0.46	0.43	0.77	0.64	0.93	0.67	0.66
<b>TiO<sub>2</sub>%</b>	0.08	0.16	0.06	0.07	0.59	0.56	0.34	0.79	0.9	0.74	0.46	0.95	0.73	0.71	0.58	0.76
<b>Total</b>	99.09	99.53	99.46	99.32	99.26	99.44	99.51	99.01	99.7	99.7	99.42	99.9	99.37	99.24	99	99.79

### 7.1.2 Pyroxene: Types and Origin

Ca-rich (Di-Fs-Hd) pyroxene series is identified by the SEM-EDX analysis in the gabbro-diorite and dioritic rock units in Washapi Kaur intrusion (Fig. 10 c, e, Table. 2). The complete solid solution between  $\text{CaMgSi}_2\text{O}_6$ - $\text{CaMgFeSi}_2\text{O}_6$ - $\text{CaFe}_2\text{Si}_2\text{O}_6$  forms the Ca-rich Diopside-Ferrosalite-Hedenbergite pyroxene series. Aluminum is poor constituent in diopsides and ferrosalite type pyroxene ( $\text{CaMgSi}_2\text{O}_6$ ), and typically, aluminum is enriched in the hedenbergite type of pyroxene ( $\text{CaFe}_2\text{Si}_2\text{O}_6$ ). The crystallization temperature Ca-rich pyroxene series (Di-Fs-Hd) is 1200 to 900 °C in binary system (34, 35). Ca-rich pyroxene series is chiefly crystallized with Ca-rich plagioclase (An) with approximately same temperature. Paragenesis of Ca-rich pyroxene series crystallized in the early stage of mafic type of magma, elsewhere the disposed type pyroxene is crystallized in strongly alkaline-rich magma and Hedenbergite type pyroxene is formed by the high aluminum and silica rich basic to intermediate type of magma (36, 37).

### 7.1.3 Amphibole

The SEM-EDX study of amphibole predominantly consists of Na constituents with Fe, Mg, K, Al, and Ti elements in gabbro and dioritic rock units in Washapi Kaur intrusion (Fig. 10 f, Table.2). The amphibole is highly pleochroic with brown color (Fig. 8 e, f). Amphibole from mafic magma, crystallized in shallow depth with high temperature about 900 °C (38, 39). High temperature is theoretically possible because they fall within the magmatic amphibole stability field, and their effect would explain the cores consistently higher Ti and Al (40). The constituents of Ti content in amphiboles group minerals increases with temperature and is the minute consequence of pressure. The presence of Ti element could be indicate the primary source of brown color amphiboles (41, 42). The brown color amphibole typically crystallized in the gabbro-diorite and dioritic

rock units in Washapi Kaur intrusion suggest that mafic magma crystallized before the infuse pulses of acidic magma in the magma chamber. Continuously magma quenching and cooling in the acidic type magma, green type of amphiboles common in granites.

### 7.1.4 Biotite

In petrographic study identified the two types of biotite (Green biotite and Brown biotite) concerning their physical properties; furthermore, in SEM-EDX compositional variation from the gabbro-diorite, diorite and granite rock units in the Washapi Kaur intrusion. The green biotite chiefly consists of magnesium (Mg), and the brown biotite mainly consists of iron (Fe) (Fig. 8 g, h and Fig. 9 g, Table. 2). Magnesium (Mg) rich biotite associated with gabbro-diorite and iron (Fe) rich biotite is with diorite and granites. The Mg enrichment in mafic-intermediate magmas indicates these rocks formed from early mafic rocks, while the Fe-rich biotite indicates the substantial subduction inputs and subsequent felsic magmatism in Washapi Kaur enriched the Fe-contents in magma.

**Table 2.** Elements mass % of rock forming minerals from Washapi Kaur Complex, Ras-Koh arc.

Sample#	Minerals	O (Mass %)	Si (Mass %)	Al (Mass %)	K (Mass %)	Na (Mass %)	Fe (Mass %)	Mg (Mass %)	Ca (Mass %)	Ti (Mass %)	Mn (Mass %)
Wk- 01.2	Amphibole	56.34	16.26	5.55	1.09	1.45	8.31	4.84	5.34	0.52	0.28
Wk- 01.3		55.6	17.81	12.24	0.49	2.13	2.9	1.44	6.88	0.18	
WK- 01.4		56.34	16.26	5.55	1.09	1.45	8.31	4.84	5.34	0.52	0.28
WK- 03.2		40.9	18.88	9.64	7.76	0.97	11.78	7.31		0.99	
WK- 03.3		44.94	11.95	6.8	3.055	2.37	4.87	2.84	1.68	0.4	
WK- 10.4		48.63	17.65	8.37	6.43	1.53	7.56	8.19		1.65	
WK- 11.3		37.53	18.95	8.33	8.62	4.15	12.93	7.38		1.84	
WK- 11.4		51.58	14.68	8.88	1.47	3.25	8.76	9.3	1.53	0.55	
WK- 15.6		51.09	21.15	6.4	4.87	1.02	5.86	7.51	1.55	0.55	
WK- 19.1		18.79	8.64	3.68	0.47	1.43	45.77	1.5	10.36	7.95	
WK- 03.1	Biotite	37.82	16.42	4.31	1.55	1.38	35.09	1.45	0.97		
WK- 03.4		43.28	14.14	7.95	3.32	1.96	21.42	7.47			
WK- 10.4		48.63	17.65	8.37	6.43	1.53	7.56	8.19			
WK- 11.3		37.53	18.95	8.33	8.62	4.15	12.93	7.38			
WK- 15.2		59.69	27.19	0.35		0.52	0.84	0.26			
WK- 15.3		51.84	12.66	10.57			15.52	9.41			
WK- 15.5		51.98	13.7	10.48	1.47	1.69	11.23	9.28			
WK- 19.2		52.96	20.41	15.11	6.59	1.82	2.09	1.03			
WK- 19.3		50.58	20.71	17.35	7.87	0.46	2.03	0.21			
WK- 19.4		53.48	20.48	14.95	6.45	1.87	2.2	0.57			
WK- 10.2	Clinopyroxer	52.28	21.08	1.32		0.63	4.99	6.86	12.49		
WK- 10.5		32.34	3.87	1.13	0.55	1.9	55.81	1.56	2.85		
WK- 11.2		52.16	20.26	2.04		0.45	5.91	7.61	11.56		
WK- 11.4		51.58	14.68	8.88	1.47	3.25	8.76	9.3	1.53		
Wk- 13.2		56.73	19.95	0.84		0.64	4.05	7.22	10.57		
WK- 13.3		48.56	23.19	1.3		0.47	4.72	7.29	14.25		
WK- 13.4		49.6	22.74	0.85			5.57	6.76	14.19		
WK- 10.8	Plagioclase	54.73	21.82	13.39		4.05			6.01		
WK- 10.11		27.35	39.05	16.46		3.62	2.15	0.13	11.24		
WK- 10.9		57.16	20.86	12.31	0.26	4.91			4.49		
WK- 15.1		48.86	25.6	15.01	2.33	4.15	0.49	0.22	3.34		
WK- 10.8		54.73	21.82	13.39		4.05			6.01		
WK- 10.6		61.02	19.72	10.64		6.15			2.48		
WK- 01.5		59.87	19.81	10.99	0.35	5.19			3.48		

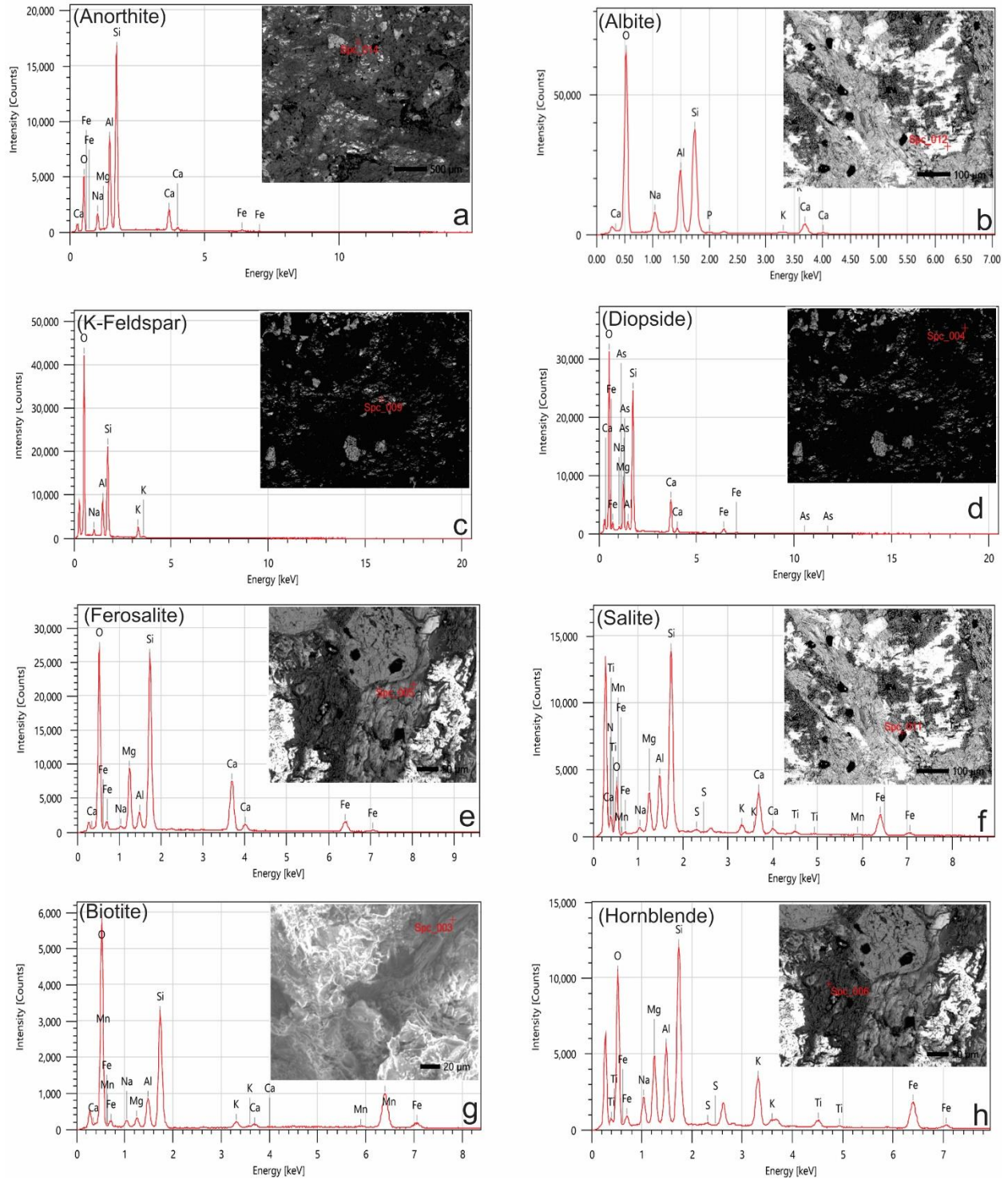


**Figure 10.** (a-h) SEM-EDX and BSE image showing the numerous rock forming mineral elemental composition of Gabbro-diorite, Diorite and Granite rock units in Washapi Kaur intrusions. (a – c) Plagioclase series (An – Alb - Kfs); (d – f) Pyroxene series (Di – Hd); (g) Biotite; (h) Hornblende.

## CONCLUSIONS

1. Washapi Kaur Intrusion intruded within the older Cretaceous Kuchaki Formation sequences are composed of gabbro-diorite, diorite, and granite.

2. The mineralogical composition of gabbro-diorites is clinopyroxene, calcium-rich plagioclase (anorthite), amphibole, and biotite. Major constituents of diorite rock units are predominantly composed of quartz, plagioclase, k-feldspar, biotite and amphibole with minor constituents of clinopyroxene. Granitic rocks consist of quartz, k-feldspar, albite plagioclase, biotite and muscovite.

3. The compositional variations in feldspar, clinopyroxene, and biotite depict the magma evolution from the oceanic-arc environment to the island arc setting.

4. The gabbro-diorite and diorite rock represent oceanic island arc and granitic rock are continental calc-alkaline arc origin.

**Conflicts of interest/Competing interests:** The authors declare no any conflict of interest/competing interests.

### Authors' contributions:

**Jafer Iqbal:** Field investigation, sampling, data processing, map drawing and draft writing. **Inayat Ullah:** Program designing, draft writing, revision. **Razzaq Abdul Manan:** Conceptualization, revision and editing. **Abdul Ghaffar:** Field investigation, Draft writing, revision and editing. **Fida Murad:** Laboratory Analysis, Draft writing, Raw data acquisition and data processing. **Jalil Ahmed:** Field investigation and sampling, draft writing.

## REFERENCES

[1] Lehmann, B. Metallogeny of tin. Springer (Vol. 32) (2006).

[2] Tabbone, Salvatore, Laurent Wendling, and J-P. Salmon. "A new shape descriptor defined on the Radon transform." *Computer Vision and Image Understanding* 102.1 (2006): 42-51.

[3] Bachmann, Olivier, and Christian Huber. "Silicic magma reservoirs in the Earth's crust." *American Mineralogist* 101.11 (2016): 2377-2404.

[4] Jellinek, A. Mark, and Donald J. DePaolo. "A model for the origin of large silicic magma chambers: precursors of caldera-forming eruptions." *Bulletin of Volcanology* 65.5 (2003): 363-381.

[5] Słaby, E., and Hervé Martin. "Mafic and felsic magma interaction in granites: the Hercynian Karkonosze Pluton (Sudetes, Bohemian Massif)." *Journal of Petrology* 49.2 (2008): 353-391.

[6] Ruprecht, Philipp, et al. "The crustal magma storage system of Volcán Quizapu, Chile, and the effects of magma mixing on magma diversity." *Journal of Petrology* 53.4 (2012): 801-840.

[7] Kennedy, Ben M., et al. "Volcanic and igneous plumbing systems of caldera volcanoes." *Volcanic and Igneous Plumbing Systems*. Elsevier, (2018). 259-284.

[8] Gao, Xue-Quan, et al. "Constraints of magmatic oxidation state on mineralization in the Beiya alkali-rich porphyry gold deposit, western Yunnan, China." *Solid Earth Sciences* 2.3 (2017): 65-78.

[9] Brown, Michael, and Tim Johnson. "Secular change in metamorphism and the onset of global plate tectonics." *American Mineralogist: Journal of Earth and Planetary Materials* 103.2 (2018): 181-196.

[10] Clemens, J. D., et al. "Mafic schlieren, crystal accumulation and differentiation in granitic magmas: an integrated case study." *Contributions to Mineralogy and Petrology* 175.5 (2020): 1-21.

[11] Nicholson, K. N., M. Khan, and K. Mahmood. "Geochemistry of the Chagai-Raskoh arc, Pakistan: Complex arc dynamics spanning the Cretaceous to the Quaternary." *Lithos* 118.3-4 (2010): 338-348.

[12] Perelló, José, Abdul Razique, and John Schloderer. "The Chagai porphyry copper belt, Baluchistan province,

- Pakistan." *Economic Geology* 103.8 (2008): 1583-1612.
- [13] Jones, A. Reconnaissance geology of part of West Pakistan: A Colombo Plan Cooperative Project. Toronto, Canada: Hunting Survey Corporation Report (1961).
- [14] Ullah, Inayat, et al. "Petrological and geochemical characterization of metamorphic sole rocks beneath the Ras Koh ophiolite, western Pakistan: Implication for a Late Cretaceous supra-subduction zone-type forearc." *Geological Journal* 56.11 (2021): 5673-5690.
- [15] Siddiqui, Rehanul Haq, M. Qasim Jan, and M. Asif Khan. "Petrogenesis of late Cretaceous lava flows from a Ceno-Tethyan island arc: The Raskoh arc, Balochistan, Pakistan." *Journal of Asian Earth Sciences* 59 (2012): 24-38.
- [16] Gnos, Edwin, et al. "Age and tectonic setting of the Ras Koh ophiolites, Pakistan." *Acta Mineralogica Pakistanica* 11 (2001): 105-118.
- [17] Arthurton, S. R. "Geological history of the Alamreg-Mashki Chah Area, Chagai District, Balochistan." *Geodynamics of Pakistan* (1979): 325-331.
- [18] Arthurton, Russell S., Abul Farah, and Wahiduddin Ahmed. "The Late Cretaceous-Cenozoic history of western Baluchistan Pakistan—the northern margin of the Makran subduction complex." *Geological Society, London, Special Publications* 10.1 (1982): 373-385.
- [19] Farah, Abul, et al. "Evolution of the lithosphere in Pakistan." *Tectonophysics* 105.1-4 (1984): 207-227.
- [20] McCormick, George R. "Geology of the Baluchistan (Pakistan) portion of the southern margin of the Tethys Sea." *Tectonic Evolution of the Tethyan Region*. Springer, Dordrecht, (1989). 277-288.
- [21] Siddiqui, R. H. "Magmatic evolution of Chagai-Raskoh arc terrane and its implication for porphyry copper mineralization." *Geologica* 2 (1996): 87-119.
- [22] Siddiqui, Rehanul Haq, Takahito Naka, and Imdad Ali Brohi. "Early To Middle Jurassic Radiolarian Fauna from the Ras Koh Arc and Its Tectonostratigraphic Significance." *Sindh University Research Journal-SURJ (Science Series)* 41.1 (2009).
- [23] Gill, R. "Igneous rocks and processes: A practical guide, Willey." (2010).
- [24] Le Maitre, Roger Walter. "A classification of igneous rocks and glossary of terms." *Recommendations of the international union of geological sciences subcommission on the systematics of igneous rocks* 193 (1989).
- [25] Peccerillo, Angelo, and S. R. Taylor. "Geochemistry of Eocene calc-alkaline volcanic rocks from the Kastamonu area, northern Turkey." *Contributions to mineralogy and petrology* 58.1 (1976): 63-81.
- [26] Castro, A., and T. V. Gerya. "Magmatic implications of mantle wedge plumes: Experimental study." *Lithos* 103.1-2 (2008): 138-148.
- [27] Kumar, Santosh. "Mafic to hybrid microgranular enclaves in the Ladakh batholith, northwest Himalaya: Implications on calc-alkaline magma chamber processes." *Journal of the Geological Society of India* 76.1 (2010): 5-25.
- [28] Ridolfi, Filippo, and Alberto Renzulli. "Calcic amphiboles in calc-alkaline and alkaline magmas: thermobarometric and chemometric empirical equations valid up to 1,130° C and 2.2 GPa." *Contributions to Mineralogy and Petrology* 163.5 (2012): 877-895.
- [29] Moyen, Jean-François, and Oscar Laurent. "Archaean tectonic systems: a view from igneous rocks." *Lithos* 302 (2018): 99-125.
- [30] Castro, A. "Plagioclase morphologies in assimilation experiments. Implications for disequilibrium melting in the generation of granodiorite rocks." *Mineralogy and Petrology* 71.1 (2001): 31-49.
- [31] Janoušek, Vojtěch, et al. "Magma-mixing in the genesis of Hercynian calc-alkaline granitoids: an integrated petrographic and

geochemical study of the Sázava intrusion, Central Bohemian Pluton, Czech Republic." *Lithos* 78.1-2 (2004): 67-99.

[32] Johnson, Breck R., and Allen F. Glazner. "Formation of K-feldspar megacrysts in granodioritic plutons by thermal cycling and late-stage textural coarsening." *Contributions to Mineralogy and Petrology* 159.5 (2010): 599-619.zl

[33] Ackerson, Michael R., et al. "Low-temperature crystallization of granites and the implications for crustal magmatism." *Nature* 559.7712 (2018): 94-97.

[34] Nimis, Paolo, and Wayne R. Taylor. "Single clinopyroxene thermobarometry for garnet peridotites. Part I. Calibration and testing of a Cr-in-Cpx barometer and an enstatite-in-Cpx thermometer." *Contributions to Mineralogy and Petrology* 139.5 (2000): 541-554.

[35] Holland, T. J. B., and R. Powell. "An improved and extended internally consistent thermodynamic dataset for phases of petrological interest, involving a new equation of state for solids." *Journal of metamorphic Geology* 29.3 (2011): 333-383.

[36] Weng, Yi-Hua, and Dean C. Presnall. "The system diopside–forsterite–enstatite at 5.1 GPa: A ternary model for melting of the mantle." *The Canadian Mineralogist* 39.2 (2001): 299-308.

[37] Dasgupta, Soumitra, and Alok K. Gupta. "The Forsterite–Diopside–Silica System at 7 Gpa And Its Significance in the Melting Behavior of the Mantle." *The Canadian Mineralogist* 50.5 (2012): 1243-1253.

[38] Blundy, Jonathan D., and Timothy JB Holland. "Calcic amphibole equilibria and a new amphibole-plagioclase geothermometer." *Contributions to mineralogy and petrology* 104.2 (1990): 208-224.

[39] Anderson, J. Lawson, and Diane R. Smith. "The effects of temperature and f O<sub>2</sub> on the Al-in-hornblende barometer." *American Mineralogist* 80.5-6 (1995): 549-559.

[40] Molina, José F., et al. "High-Ti amphibole as a petrogenetic indicator of magma chemistry: evidence for mildly alkalic-hybrid melts during evolution of Variscan basic–ultrabasic magmatism of Central Iberia." *Contributions to Mineralogy and Petrology* 158.1 (2009): 69-98.

[41] Zhang, S. H., Y. Zhao, and B. Song. "Hornblende thermobarometry of the Carboniferous granitoids from the Inner Mongolia Paleo-uplift: implications for the tectonic evolution of the northern margin of North China block." *Mineralogy and Petrology* 87.1 (2006): 123-141.

[42] Terentiev, R. A., and K. A. Savko. "Paleoproterozoic high-Mg low-Ti gabbro-granite series in eastern Sarmatia: geochemistry and formation conditions." *Russian Geology and Geophysics* 57.6 (2016): 907-932.

Received: 17 Feb. 2022. Revised/Accepted: 24 March 2022.



This work is licensed under a Creative Commons Attribution 4.0 International License.

---